Available online at www.sciencedirect.com
ScienceDirect
Journal of Sound and Vibration 298 (2006) 366–384
JOURNAL OF SOUND AND VIBRATION
www.elsevier.com/locate/jsvi

Structural modification of a helicopter tailcone

John E. Mottershead*, Maryam Ghandchi Tehrani, Danut Stancioiu[1], Simon James, Hossein Shahverdi

Department of Engineering, The University of Liverpool, Liverpool L69 3GH, UK

Received 11 January 2006; received in revised form 13 April 2006; accepted 23 May 2006
Available online 8 August 2006

Abstract

The structural modification of a Lynx Mark 7 helicopter tailcone is considered. The problem is especially demanding because of the almost symmetric structure of the tailcone, which in its initial configuration (prior to modification) results in a number of very weakly excited responses to certain excitations, so the corresponding terms in the full 6×6 receptance matrix are very difficult to obtain. The modification, in the form of a large overhanging mass, has the effect of coupling the initial-system responses and the weakly excited ones become important in determining the modified-system receptances using the structural-modification theory. The results are interpreted with the aid of a finite-element model. Very good estimates of the rotational receptances are obtained, the only significant difference from finite-element results being that the model is stiffer than the physical structure. Noise on the weakly exited responses is amplified in the estimated modified-system responses and it is demonstrated, using the finite-element model, that the use of a single X-block measurement to connect the modification to the tailcone is insufficient at frequencies higher than the first double peak of the modified-system receptances. It is considered that the exercise provides a demanding test of structural modification theory resulting in a very useful practical assessment of the limitations of the method.

1. Introduction

The problem of determining the effects of a known modification on an existing structure with measured dynamic behaviour is a *Structural Modification* problem. The principles of structural modification are long established; in 1941 Duncan [1] determined the behaviour of a compound system formed from two or more subsystems, each with measured receptances, and known interconnection properties. Bishop and Johnson [2] described the receptance method eloquently and in detail, and Ewins [3] described applications of structural modification in modern modal analysis. Mottershead and Ram [4] considered the inverse problem of determining the passive modification (and alternatively the active control) necessary to assign selected eigenvalues (poles and zeros) to a dynamic system.

In practice, several problems arise when applying structural modification theory to measured data. Small measurement inaccuracies can lead to large discrepancies in the estimated modified-system receptances at

*Corresponding author.
E-mail address: j.e.mottershead@liv.ac.uk (J.E. Mottershead).
[1]Now with the Acoustic Research Centre, University of Salford, UK.

0022-460X/$ - see front matter © 2006 Elsevier Ltd. All rights reserved.
doi:10.1016/j.jsv.2006.05.026

frequencies close to the natural frequencies of the initial system. It was shown [5] for the rank-1 modification that this problem occurs because of polynomials in the numerator and denominator of the modified receptances that should cancel precisely at the poles of the initial system. In the case of perfect data, such as simulated data with zero measurement noise, the cancellation is exact, but measurements from physical systems inevitably contain noise so that the cancellation fails to occur even when the measurements contain the slightest inaccuracy. The effect is to produce a characteristic equation in the denominator with eigenvalues at the poles of both the original and modified systems. This problem occurs only when the measurement coordinates and the modification attachment coordinates are different and cannot be corrected by removing small singular values from the receptance matrix, as has often been tried unsuccessfully. Another problem with practical modifications, such as added beams or large masses, is that rotational coordinates are required to connect the modification to the initial structure. This necessitates the measurement of rotational receptances, which is difficult and requires specialist skills. Essentially, there are two approaches: (1) apply a pure moment and measure the resulting rotation or (2) apply a force that simultaneously imparts a moment to the structure and then from measured linear acceleration responses determine a matrix of receptances using a multiple-input, multiple-output estimator. A review of rotational receptance techniques extending to 34 references is included in the Introduction to [6], which goes on to describe various problems of ill-conditioning brought about by the assumption of rigidity of the attachment used to deliver a moment at the connection point. The ill-conditioning problem may be greatly alleviated by allowing flexibility of the attachment, in which case a model of the attachment must be included in the formulation of the estimator, as described in [6]. In [7] the inverse problem of determining the sectional properties of a beam in order assign natural frequencies and antiresonances to a portal frame structure using the rotational receptance measurements described in [6] was considered.

In this paper, the modification of a Westland Mark 7 Lynx helicopter tailcone is described. Estimates of the full 6×6 receptance matrix are determined using an X-block attachment. Flexibility of the attachment is included in the formulation of H_1 and H_2 estimators [8] so that the arms and stem of the attachment may be long enough to impart a significant moment at the connection point. The baseline tailcone is almost, but not quite, symmetric and the modification is a large overhanging mass at the top of the pylon, representative of the mass and inertia of the tail rotor gearbox and hub. Certain initial-system responses are excited only very weakly because of the near-symmetry of the baseline tailcone. The full 6×6 matrix of receptances is therefore especially difficult to estimate, but the overhanging mass and inertia couples all the initial-system receptances in determining the dynamic behaviour of the modified system. Estimated rotational receptances of the initial- and modified-system receptances are compared to results obtained from a finite-element model. The modified-system receptances, determined from initial-system measurements and the known inertia matrix of the modification, are compared to finite-element predictions and also to measurements carried out on the tailcone with the overhanging mass modification.

2. Estimation of rotational receptances

The theory for estimating the rotational receptances of a T-block attachment is described in [6]. This device enables the estimation of an in-plane 3×3 receptance matrix at two linear coordinates and one rotational coordinate. It is not possible to determine a full 6×6 matrix using T-bocks alone. Use of the X-block, shown in Fig. 1, however enables the estimation a 5×5 matrix of receptances, and by moving the X-block into different positions the full 6×6 matrix may be obtained. The local X-block coordinate system shown in the figure is used in the formulation of the multiple-input, multiple-output estimator of the 5×5 receptance matrix at each position of the X-block.

We begin, as in [6], by writing the equation of motion of the system with the attached X-block,

$$\begin{bmatrix} \mathbf{B}_{11}(\omega) & \mathbf{B}_{10}(\omega) & \mathbf{0} \\ \mathbf{B}_{01}(\omega) & \mathbf{B}_{00}(\omega) & \mathbf{0} \\ \mathbf{0} & \mathbf{0} & \mathbf{0} \end{bmatrix} \begin{pmatrix} \mathbf{x}_1 \\ \mathbf{x}_0 \\ \mathbf{x}_2 \end{pmatrix} = \begin{pmatrix} \mathbf{0} \\ \mathbf{f}_0 \\ \mathbf{f}_2 \end{pmatrix} - \begin{bmatrix} \mathbf{0} & \mathbf{0} & \mathbf{0} \\ \mathbf{0} & \tilde{\mathbf{B}}_{00}(\omega) & \tilde{\mathbf{B}}_{02}(\omega) \\ \mathbf{0} & \tilde{\mathbf{B}}_{20}(\omega) & \tilde{\mathbf{B}}_{22}(\omega) \end{bmatrix} \begin{pmatrix} \mathbf{x}_1 \\ \mathbf{x}_0 \\ \mathbf{x}_2 \end{pmatrix}, \tag{1}$$

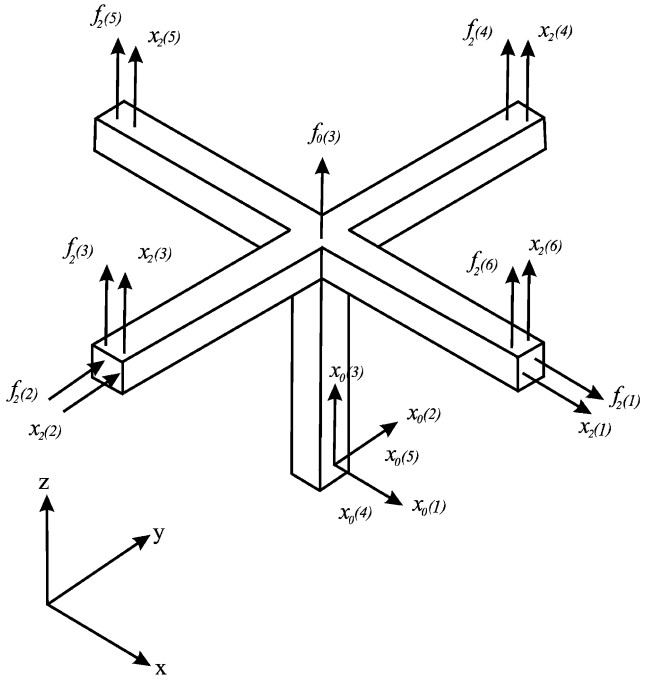

Fig. 1. X-block forces and displacements.

where the subscripts 0, 1, 2 denote the shared structure/X-block connection-point coordinates, the coordinates of the structure (excluding the connection point) and the X-block coordinates (excluding the connection point), respectively. The submatrices $\mathbf{B}_{11}(\omega)$, $\mathbf{B}_{01}(\omega)$, $\mathbf{B}_{00}(\omega)$ are unknown dynamic stiffnesses of the structure and $\tilde{\mathbf{B}}_{00}(\omega)$, $\tilde{\mathbf{B}}_{20}(\omega)$, $\tilde{\mathbf{B}}_{22}(\omega)$ are X-block dynamic stiffnesses determined from a finite-element model.

Fig. 1 shows the measured forces $\mathbf{f}_0(\omega)$ and $\mathbf{f}_2(\omega)$, the measured displacements $\mathbf{x}_2(\omega)$ (obtained from accelerometer measurements) and the unmeasured displacements $\mathbf{x}_0(\omega)$ defined in the local X-block coordinate system used in the following theory. The dimensions of the force and displacement vectors are as follows:

$$\mathbf{f}_0 \in C^{5\times 1}, \quad \mathbf{f}_2 \in C^{6\times 1}, \quad \mathbf{x}_2 \in C^{6\times 1}, \quad \mathbf{x}_0 \in C^{5\times 1}, \tag{2}$$

where C denotes the set of complex numbers. The forces $\mathbf{f}_2(1)\ldots\mathbf{f}_2(6)$ and $\mathbf{f}_0(3)$ are applied consecutively in seven separate tests, so that for example, in the first test $\mathbf{f}_0$ is the null vector and only the first term in $\mathbf{f}_2$ is non-zero ($\mathbf{f}_0(i) = 0,\ i = 1, 2, \ldots, 5$ and $\mathbf{f}_2(i) = 0,\ i = 2, 3, \ldots, 6$).

Eq. (1) may be separated into two parts,

$$\begin{bmatrix} \mathbf{B}_{11}(\omega) & \mathbf{B}_{10}(\omega) \\ \mathbf{B}_{01}(\omega) & \mathbf{B}_{00}(\omega) \end{bmatrix} \begin{pmatrix} \mathbf{x}_1 \\ \mathbf{x}_0 \end{pmatrix} = \begin{pmatrix} \mathbf{0} \\ \mathbf{f}_0 - \left(\tilde{\mathbf{B}}_{00}(\omega)\mathbf{x}_0 + \tilde{\mathbf{B}}_{02}(\omega)\mathbf{x}_2\right) \end{pmatrix} \tag{3}$$

and

$$\mathbf{f}_2 - \left(\tilde{\mathbf{B}}_{20}(\omega)\mathbf{x}_0 + \tilde{\mathbf{B}}_{22}(\omega)\mathbf{x}_2\right) = 0. \tag{4}$$

The receptance matrix of the parent structure without the X-block is not measured directly but is defined as the inverse of the unknown dynamic stiffness matrix,

$$\begin{bmatrix} \mathbf{H}_{11}(\omega) & \mathbf{H}_{10}(\omega) \\ \mathbf{H}_{01}(\omega) & \mathbf{H}_{00}(\omega) \end{bmatrix} = \begin{bmatrix} \mathbf{B}_{11}(\omega) & \mathbf{B}_{10}(\omega) \\ \mathbf{B}_{01}(\omega) & \mathbf{B}_{00}(\omega) \end{bmatrix}^{-1}. \tag{5}$$

Our objective is to determine the receptance submatrix $\mathbf{H}_{00}(\omega)$ and an expression in this term alone can be obtained from Eq. (3) after premultiplying by the matrix defined in Eq. (5). Then the second row of the

resulting matrix equation gives,

$$\mathbf{x}_0 = \mathbf{H}_{00}(\omega)\big(\mathbf{f}_0 - \big(\tilde{\mathbf{B}}_{00}(\omega)\mathbf{x}_0 + \tilde{\mathbf{B}}_{02}(\omega)\mathbf{x}_2\big)\big). \tag{6}$$

Eliminating the unmeasured $\mathbf{x}_0$ by combining Eqs. (6) and (4) leads to,

$$\begin{aligned}\Big(\tilde{\mathbf{B}}_{20}^{*\mathrm{T}}(\omega)\tilde{\mathbf{B}}_{20}(\omega)\Big)^{-1}\tilde{\mathbf{B}}_{20}^{*\mathrm{T}}(\omega)\big(\mathbf{f}_2 - \tilde{\mathbf{B}}_{22}(\omega)\mathbf{x}_2\big) &= \mathbf{H}_{00}(\omega)\\ \times\left(\mathbf{f}_0 - \Big(\tilde{\mathbf{B}}_{20}^{*\mathrm{T}}(\omega)\tilde{\mathbf{B}}_{20}(\omega)\Big)^{-1}\tilde{\mathbf{B}}_{20}^{*\mathrm{T}}(\omega)\big(\mathbf{f}_2 - \tilde{\mathbf{B}}_{22}(\omega)\mathbf{x}_2\big) + \tilde{\mathbf{B}}_{02}(\omega)\mathbf{x}_2\right),\end{aligned} \tag{7}$$

where the finite-element dynamic stiffness submatrices have the following dimensions,

$$\tilde{\mathbf{B}}_{20}(\omega) \in C^{6\times 5}, \quad \tilde{\mathbf{B}}_{00}(\omega) \in C^{5\times 5}, \quad \tilde{\mathbf{B}}_{22}(\omega) \in C^{6\times 6} \tag{8}$$

and the asterisk denotes complex conjugation. Eq. (7) may be re-written in the simplified form,

$$\mathbf{R}(\omega)\mathbf{f}_2(\omega) + \mathbf{S}(\omega)\mathbf{x}_2(\omega) = \mathbf{H}_{00}(\omega)(\mathbf{f}_0(\omega) + \mathbf{T}(\omega)\mathbf{f}_2(\omega) + \mathbf{U}(\omega)\mathbf{x}_2(\omega)) \tag{9}$$

or

$$\begin{bmatrix}\mathbf{R}(\omega) & \mathbf{S}(\omega)\end{bmatrix}\begin{pmatrix}\mathbf{f}_2(\omega)\\ \mathbf{x}_2(\omega)\end{pmatrix} = \mathbf{H}_{00}\begin{bmatrix}\mathbf{I} & \mathbf{T}(\omega) & \mathbf{U}(\omega)\end{bmatrix}\begin{pmatrix}\mathbf{f}_0(\omega)\\ \mathbf{f}_2(\omega)\\ \mathbf{x}_2(\omega)\end{pmatrix}, \tag{10}$$

where

$$\mathbf{R}(\omega) = \Big(\tilde{\mathbf{B}}_{20}^{*\mathrm{T}}(\omega)\tilde{\mathbf{B}}_{20}(\omega)\Big)^{-1}\tilde{\mathbf{B}}_{20}^{*\mathrm{T}}(\omega), \tag{11}$$

$$\mathbf{S}(\omega) = -\Big(\tilde{\mathbf{B}}_{20}^{*\mathrm{T}}(\omega)\tilde{\mathbf{B}}_{20}(\omega)\Big)^{-1}\tilde{\mathbf{B}}_{20}^{*\mathrm{T}}(\omega)\tilde{\mathbf{B}}_{22}(\omega), \tag{12}$$

$$\mathbf{T}(\omega) = -\tilde{\mathbf{B}}_{00}(\omega)\Big(\tilde{\mathbf{B}}_{20}^{*\mathrm{T}}(\omega)\tilde{\mathbf{B}}_{20}(\omega)\Big)^{-1}\tilde{\mathbf{B}}_{20}^{*\mathrm{T}}(\omega), \tag{13}$$

$$\mathbf{U}(\omega) = \tilde{\mathbf{B}}_{00}(\omega)\Big(\tilde{\mathbf{B}}_{20}^{*\mathrm{T}}(\omega)\tilde{\mathbf{B}}_{20}(\omega)\Big)^{-1}\tilde{\mathbf{B}}_{20}^{*\mathrm{T}}(\omega)\tilde{\mathbf{B}}_{22}(\omega) - \tilde{\mathbf{B}}_{02}(\omega) \tag{14}$$

are all matrices formed from the finite-element model of the X-block.

2.1. H_1 estimator

Postmultiplying both sides of Eq. (10) by

$$\begin{bmatrix}\mathbf{f}_0^{*\mathrm{T}}(\omega) & \mathbf{f}_2^{*\mathrm{T}}(\omega) & \mathbf{x}_2^{*\mathrm{T}}(\omega)\end{bmatrix}\begin{bmatrix}\mathbf{I}\\ \mathbf{T}^{*\mathrm{T}}(\omega)\\ \mathbf{U}^{*\mathrm{T}}(\omega)\end{bmatrix}$$

and taking n averages for each of the seven separate load cases leads to the expression,

$$\mathbf{B}(\omega) = \mathbf{H}_{00}(\omega)\mathbf{A}(\omega), \tag{15}$$

where

$$\mathbf{A}(\omega) = \begin{bmatrix}\mathbf{I} & \mathbf{T}(\omega) & \mathbf{U}(\omega)\end{bmatrix}\begin{bmatrix}\mathbf{G}_{f_0f_0} & \mathbf{G}_{f_0f_2} & \mathbf{G}_{f_0x_2}\\ \mathbf{G}_{f_2f_0} & \mathbf{G}_{f_2f_2} & \mathbf{G}_{f_2x_2}\\ \mathbf{G}_{x_2f_0} & \mathbf{G}_{x_2f_2} & \mathbf{G}_{x_2x_2}\end{bmatrix}\begin{bmatrix}\mathbf{I}\\ \mathbf{T}^{*\mathrm{T}}(\omega)\\ \mathbf{U}^{*\mathrm{T}}(\omega)\end{bmatrix}, \tag{16}$$

$$\mathbf{B}(\omega) = \begin{bmatrix} \mathbf{R}(\omega) & \mathbf{S}(\omega) \end{bmatrix} \begin{bmatrix} \mathbf{G}_{f_2 f_0}(\omega) & \mathbf{G}_{f_2 f_2}(\omega) & \mathbf{G}_{f_2 x_2}(\omega) \\ \mathbf{G}_{x_2 f_0}(\omega) & \mathbf{G}_{x_2 f_2}(\omega) & \mathbf{G}_{x_2 x_2}(\omega) \end{bmatrix} \begin{bmatrix} \mathbf{I} \\ \mathbf{T}^{*\mathrm{T}}(\omega) \\ \mathbf{U}^{*\mathrm{T}}(\omega) \end{bmatrix}, \tag{17}$$

and

$$\mathbf{A}(\omega),\ \mathbf{B}(\omega) \in C^{5\times 5}. \tag{18}$$

The submatrices, typically $\mathbf{G}_{f_0 x_2}(\omega)$, contain power spectal densities. For example,

$$\mathbf{G}_{f_0 x_2}(\omega) = \sum_{1}^{7} \frac{1}{n} \sum_{i=1}^{n} \begin{bmatrix} f_0^i(1)x_2^i(1) & f_0^i(1)x_2^i(2) & f_0^i(1)x_2^i(3) & f_0^i(1)x_2^i(4) & f_0^i(1)x_2^i(5) & f_0^i(1)x_2^i(6) \\ f_0^i(2)x_2^i(1) & f_0^i(2)x_2^i(2) & f_0^i(2)x_2^i(3) & f_0^i(2)x_2^i(4) & f_0^i(2)x_2^i(5) & f_0^i(2)x_2^i(6) \\ f_0^i(3)x_2^i(1) & f_0^i(3)x_2^i(2) & f_0^i(3)x_2^i(3) & f_0^i(3)x_2^i(4) & f_0^i(3)x_2^i(5) & f_0^i(3)x_2^i(6) \\ f_0^i(4)x_2^i(1) & f_0^i(4)x_2^i(2) & f_0^i(4)x_2^i(3) & f_0^i(4)x_2^i(4) & f_0^i(4)x_2^i(5) & f_0^i(4)x_2^i(6) \\ f_0^i(5)x_2^i(1) & f_0^i(5)x_2^i(2) & f_0^i(5)x_2^i(3) & f_0^i(5)x_2^i(4) & f_0^i(5)x_2^i(5) & f_0^i(5)x_2^i(6) \end{bmatrix}, \tag{19}$$

where the subscript denoting the load case is omitted for clarity. Finally the H_1 estimate is given by

$$\mathbf{H}_{00}(\omega) = \mathbf{A}^{-1}(\omega)\mathbf{B}(\omega). \tag{20}$$

2.2. H_2 estimator

When Eq. (10) is postmultiplied on both sides by

$$\begin{bmatrix} \mathbf{f}_2^{*\mathrm{T}}(\omega) & \mathbf{x}_2^{*\mathrm{T}}(\omega) \end{bmatrix} \begin{bmatrix} \mathbf{R}^{*\mathrm{T}}(\omega) \\ \mathbf{S}^{*\mathrm{T}}(\omega) \end{bmatrix},$$

then the following expression is obtained:

$$\mathbf{D}(\omega) = \mathbf{H}_{00}(\omega)\mathbf{C}(\omega), \tag{21}$$

where

$$\mathbf{C}(\omega) = \begin{bmatrix} \mathbf{I} & \mathbf{T}(\omega) & \mathbf{U}(\omega) \end{bmatrix} \begin{bmatrix} \mathbf{G}_{f_0 f_2}(\omega) & \mathbf{G}_{f_0 x_2}(\omega) \\ \mathbf{G}_{f_2 f_2}(\omega) & \mathbf{G}_{f_2 x_2}(\omega) \\ \mathbf{G}_{x_2 f_2}(\omega) & \mathbf{G}_{x_2 x_2}(\omega) \end{bmatrix} \begin{bmatrix} \mathbf{R}^{*\mathrm{T}}(\omega) \\ \mathbf{S}^{*\mathrm{T}}(\omega) \end{bmatrix}, \tag{22}$$

$$\mathbf{D}(\omega) = \begin{bmatrix} \mathbf{R}(\omega) & \mathbf{S}(\omega) \end{bmatrix} \begin{bmatrix} \mathbf{G}_{f_2 f_2}(\omega) & \mathbf{G}_{f_2 x_2}(\omega) \\ \mathbf{G}_{x_2 f_2}(\omega) & \mathbf{G}_{x_2 x_2}(\omega) \end{bmatrix} \begin{bmatrix} \mathbf{R}^{*\mathrm{T}}(\omega) \\ \mathbf{S}^{*\mathrm{T}}(\omega) \end{bmatrix} \tag{23}$$

and

$$\mathbf{C}(\omega),\ \mathbf{D}(\omega) \in C^{5\times 5}. \tag{24}$$

The H_2 estimate is then given by

$$\mathbf{H}_{00}(\omega) = \mathbf{C}^{-1}(\omega)\mathbf{D}(\omega). \tag{25}$$

3. Finite-element model of the X-block

The finite-element model of the X-block consists of five beam elements with transcendental shape functions that solve the dynamic Euler–Bernoulli beam equation exactly in the frequency domain. The beams are inextensible in tension/compression and axial torsion and the element dynamic stiffness matrix is given, for example, by Narayanan [9]. The dimensions of the X-block, manufactured in mild steel, are shown in Fig. 2

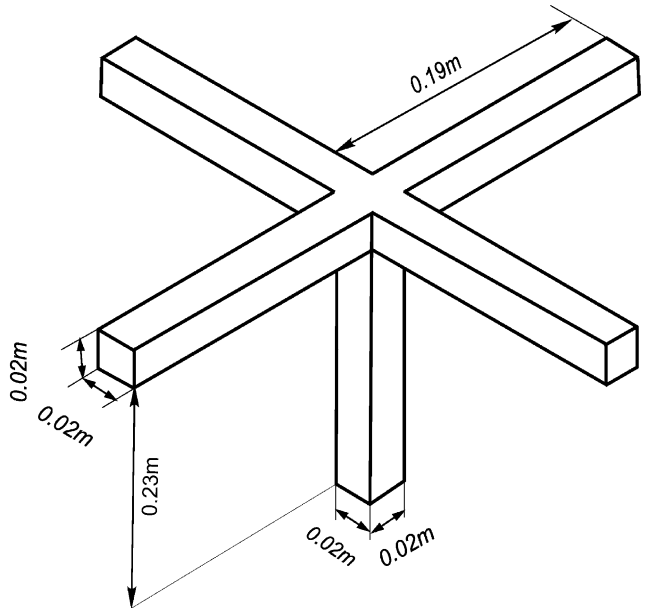

Fig. 2. X-block dimensions.

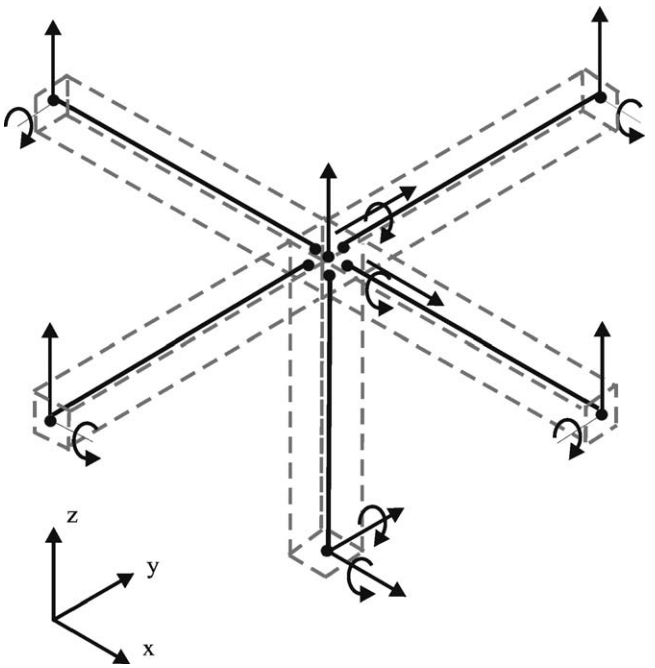

Fig. 3. X-block finite-element model.

and the finite-element model in Fig. 3. The joint between the four arms and the stem is modelled using an offset node at the intersection of the centrelines and the displacements at the connecting nodes may be determined from rigid constraints. The four rotational coordinates at the tips of the arms and the two at the joint are unmeasured and must be eliminated from the model. This is achieved by applying Guyan reduction to the assembled dynamic stiffness matrix, which is a function of frequency. Thus when a different reduction is carried out at each frequency increment the process does not incur any loss of accuracy in the reduced

dynamic stiffness matrix. Care should be taken in dealing with mass terms such the masses of the arms, which need to be added to the dynamic stiffness of the stem (at the joint) in both the local x and y coordinates. Similarly the mass of the stem needs to be added at axial coordinate $x_0(3)$.

The first natural frequencies of the finite-element model, fixed at the base of the stem, are two stem-bending modes at 61 Hz. Two corresponding frequencies at 58 and 61 Hz were found in a hammer-excited modal test, with the base fixed to a rigid heavy metal block.

4. Helicopter tailcone

The Westland Mark 7 Lynx tailcone is shown together with the global axis system (used for the presentation of results) in Fig. 4. It was detached at the transport joint and attached via an aluminium plate to a rigid wall. The tailcone is nearly, but not perfectly, symmetric about the X–Z plane. A large overhanging 76 kg mass, almost exactly the same mass as the tailcone itself and representative of the tail-rotor gearbox and hub, can be seen at the top left of the figure. The X-block attachment point, shown in Fig. 5, did not coincide exactly with the attachment of the overhanging mass.

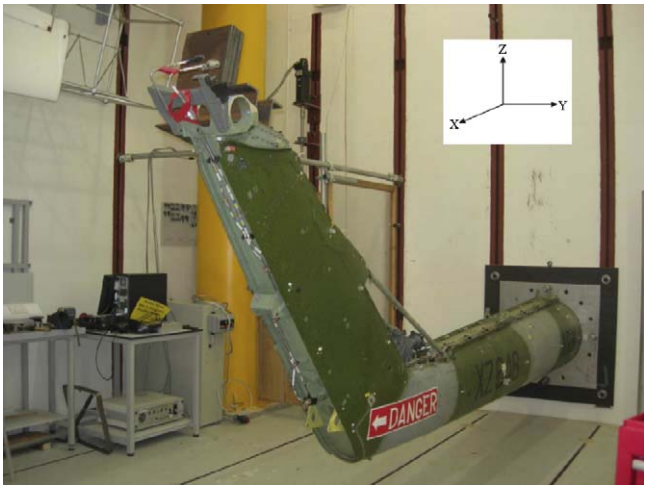

Fig. 4. Tailcone global coordinate system.

Fig. 5. X-block attached to the tailcone.

A preliminary hammer test was carried out on the baseline tailcone (without the added mass and also without the X-block). The first two vibration modes at 12.7 and 13.2 Hz showed coupling between the lateral (X–Z) and transverse (Y–Z) bending modes, the bending planes being almost perpendicular and at approximately 45° to the Y–Z axes. There was no discernable torsion about the X-axis. The third and Fourth modes at 46 and 58 Hz did however show rotation about the X-axis coupled with lateral and transverse bending. The large overhanging-mass modification was expected to introduce torsional coupling (and possibly yet more complicated coupling of displacement and rotation) even in the lowest frequency modes and therefore cross moment-rotation receptances were needed at the connection point in order to determine the dynamics of the added-mass system by the structural-modification theory. The finite-element model of the tailcone (in MSC-NASTRAN) consisted of 2771 elements (1600 nodes) including 1508 CQUAD4 elements and 1139 CBEAM elements.

5. Estimated baseline-tailcone receptances

The estimated upper triangle of the 6×6 matrix of H_1 receptance magnitudes from the X-block mounted in three mutually perpendicular orientations is given in Figs. 6–8 together with the same matrix terms determined from the finite-element model. There is some duplication of results when the X-block is mounted in the three different orientations, and of course certain configurations are best suited for the estimation of particular matrix terms. Of the duplicated estimates the least noisy ones were selected for presentation, though generally all of them were in quite reasonable agreement. The spectral densities, in Eqs. (16) and (17), were determined directly from a modal test using random excitation over the range of 0–160 Hz and 512 spectral lines. An average of 500 measurements was taken with a 32% overlap. The receptances produced from the tail-cone

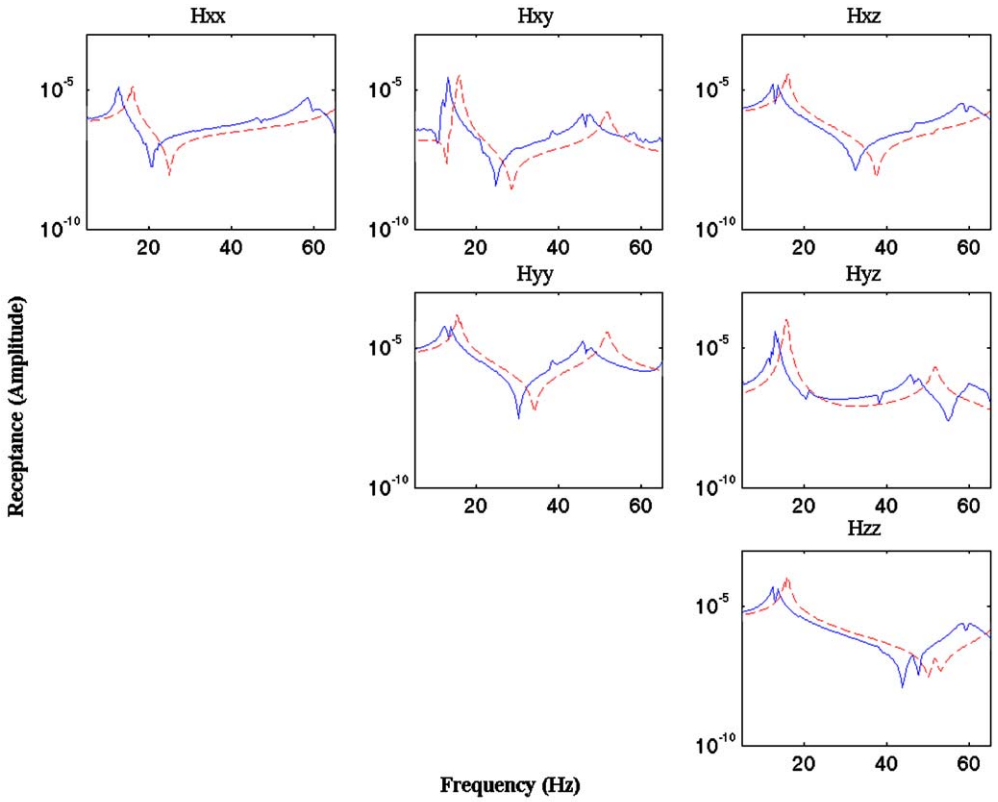

Fig. 6. Upper left-hand receptance matrix (magnitude—m/N): solid line—estimated from X-block measurements and dashed line—finite element.

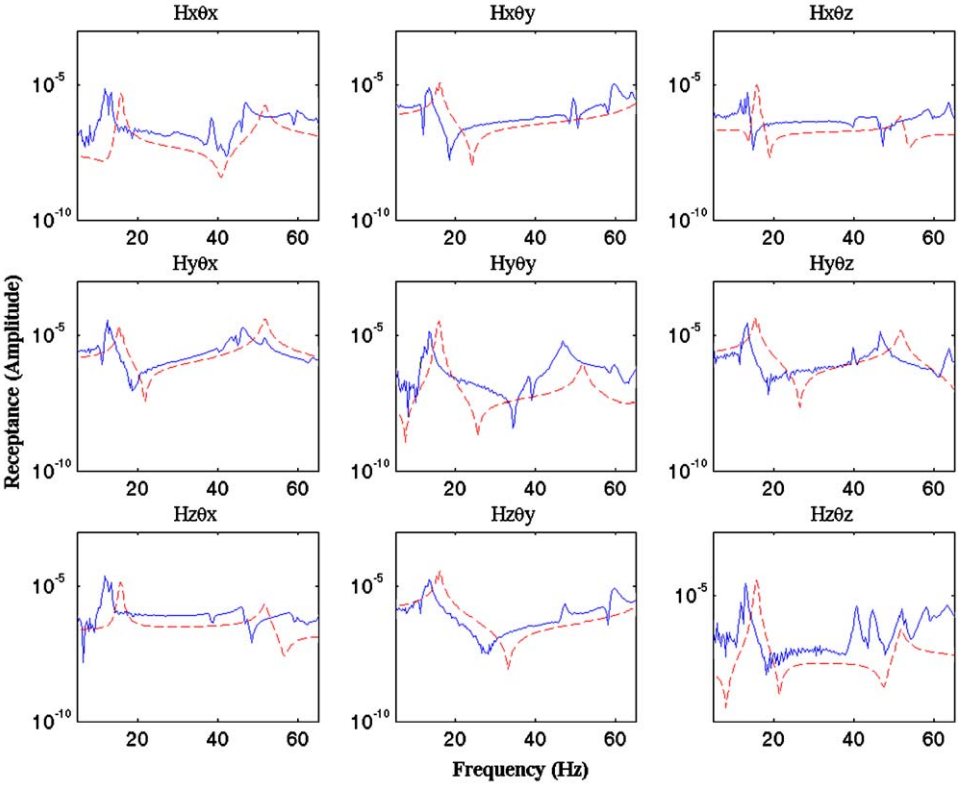

Fig. 7. Upper right-hand receptance matrix (magnitude—N^{-1}): solid line—estimated from X-block measurements and dashed line—finite element.

finite-element model were determined using modal damping at 0.1% of critical for all modes in the range 0–250 Hz.

It can be seen that the finite-element model is stiffer than the physical system. Probably the most difficult terms to estimate are the terms on the diagonal of the upper right-hand sub-matrix in Fig. 7, including the extremely difficult to obtain $H_{00}(1,4)$ representing the rotational response θ_x to the force f_x. It can be seen that the terms $H_{00}(1,4)$, $H_{00}(2,5)$ and $H_{00}(3,6)$ are amongst the most noisy estimates, yet still show good agreement with the finite-element results. The rotational receptances, shown in Fig. 8, appear to be quite different to the translational receptances we are used to seeing, being quite flat except for peaks and troughs over narrow frequency bands. Of course, it is important that not only the magnitudes but also the phases of the 6×6 matrix are accurately determined. These are shown in Figs. 9–11. The differences in the shape of the phase plots at the 180° resonance phase changes are due only to differences in the modal damping (at 0.1% of critical) applied in the finite-element model from the damping of the real structure. The H_2 estimates appear to be generally of poorer quality than the H_1 estimates as shown for example in Fig. 12.

6. Structural modification

The details of the structural-modification theory can be found in Refs. [4,7], where it is explained how the receptance of a system $\mathbf{B}(\omega)\mathbf{f}(\omega) = \mathbf{x}(\omega)$ modified by an added dynamic stiffness $\Delta\mathbf{B}(\omega)$ may be written in the form,

$$\tilde{\mathbf{H}}(\omega) = (\mathbf{I} + \mathbf{H}(\omega)\Delta\mathbf{B}(\omega))^{-1}\mathbf{H}(\omega), \tag{26}$$

where $\tilde{\mathbf{H}}(\omega)$ represents the matrix of modified-system receptances and $\mathbf{H}(\omega)$ contains the receptances of the initial system.

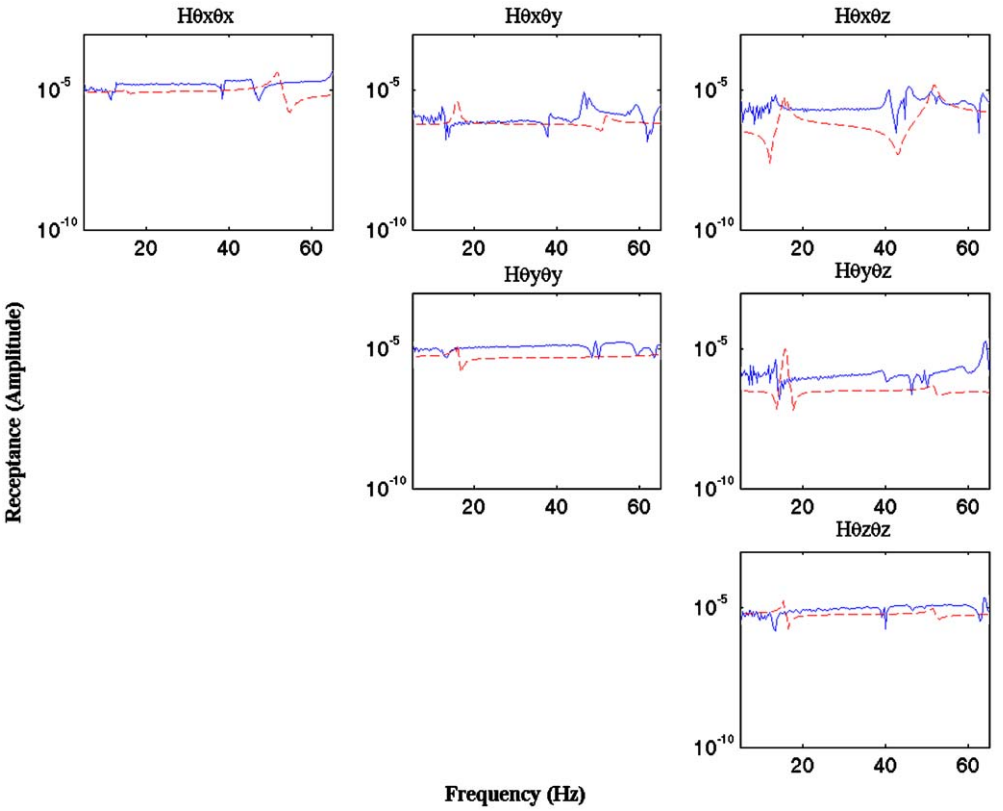

Fig. 8. Lower right-hand receptance matrix (magnitude—(N/m)): solid line—estimated from X-block measurements and dashed line—finite element.

6.1. The overhanging mass modification

The overhanging mass modification and position vector $\vec{\mathbf{r}}$ of the centre of mass with respect to the connection point of the X-block is shown in Fig. 13. The centre of gravity is denoted by '0' and the connection point by '1'. A solid model placed in position on the finite-element mesh is shown in Fig. 14. The modification consisted mainly of a solid piece of steel of dimensions $410 \times 230 \times 80$ mm and two-channel section beams, each 125 mm × 65 mm (15 mm wall thickness) × 410 mm long. The attachment was via a 15 mm mild steel plate using six 8 mm bolts connecting into the rigid tail-rotor gearbox mounting.

For the purposes of applying the modification theory it was assumed that the modification itself was rigid and could therefore be represented by its total mass and the 3×3 inertia matrix at the centre of mass. This is described by the mass modification matrix,

$$\Delta\mathbf{M} = \begin{bmatrix} 75.6 & & & & & \\ & 75.6 & & & & \\ & & 75.6 & & & \\ & & & 1.844 & -0.044 & 0.184 \\ & & & -0.044 & 1.268 & 0.254 \\ & & & 0.184 & 0.254 & 0.832 \end{bmatrix}. \tag{27}$$

The position vector that defines of the centre of mass with respect to the X-block connection point is given by

$$\vec{\mathbf{r}} = -0.256\mathbf{i} - 0.213\mathbf{j} + 0.209\mathbf{k}. \tag{28}$$

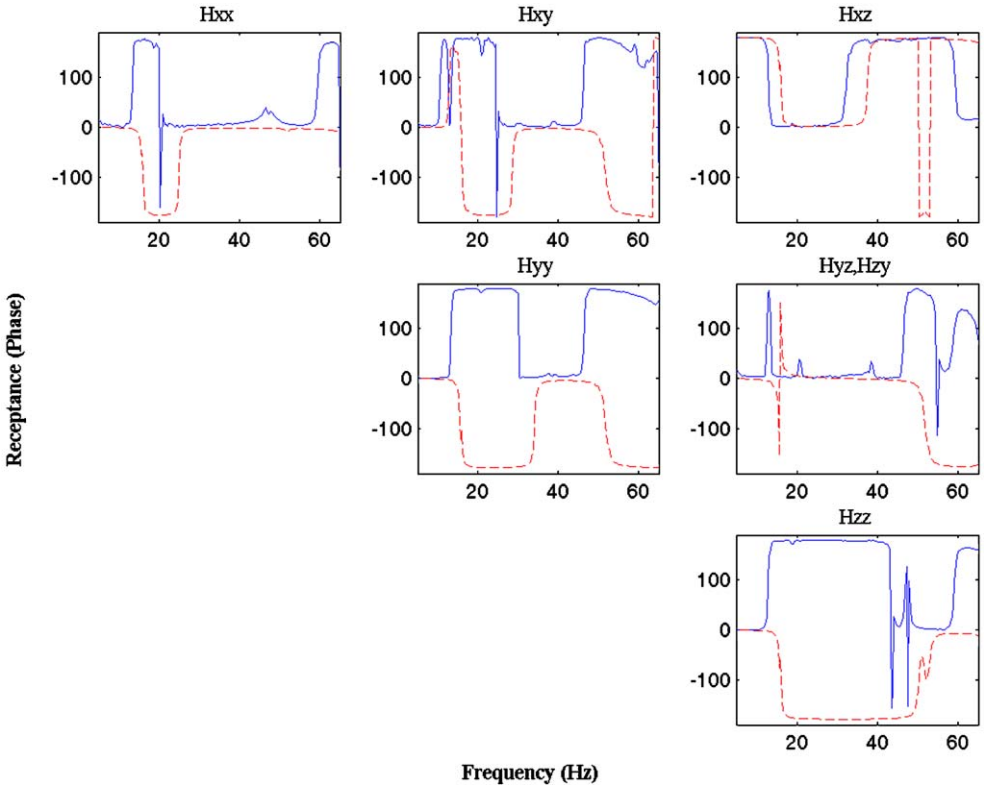

Fig. 9. Upper left-hand receptance matrix (phase): solid line—estimated from X-block measurements and dashed line—finite element.

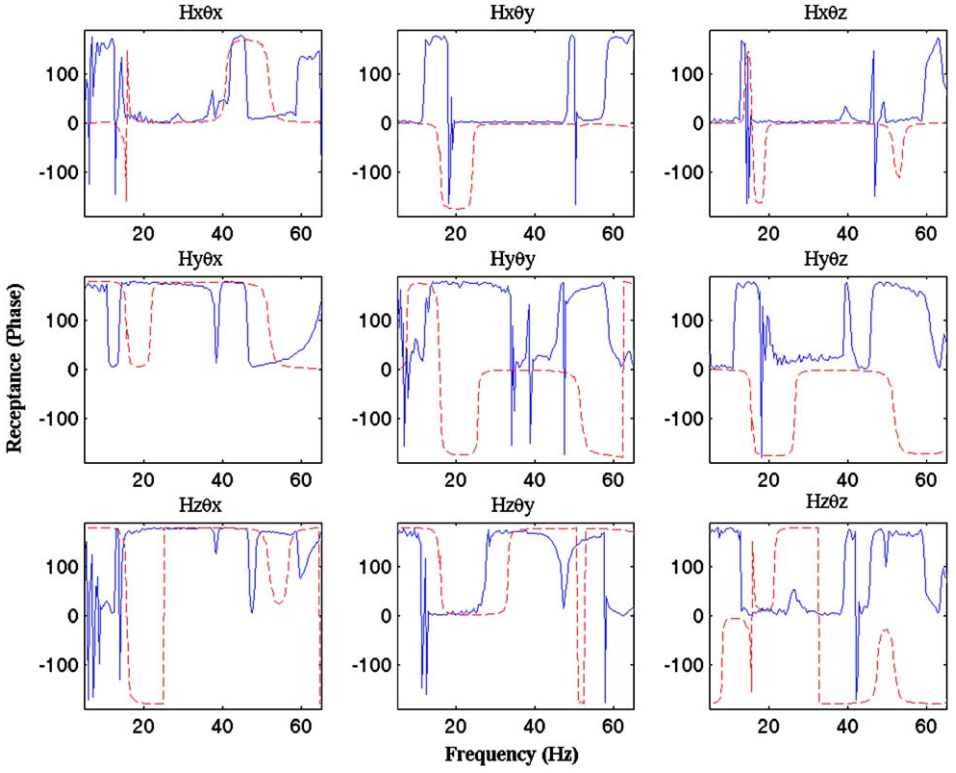

Fig. 10. Upper right-hand receptance matrix (phase): solid line—estimated from X-block measurements and dashed line—finite element.

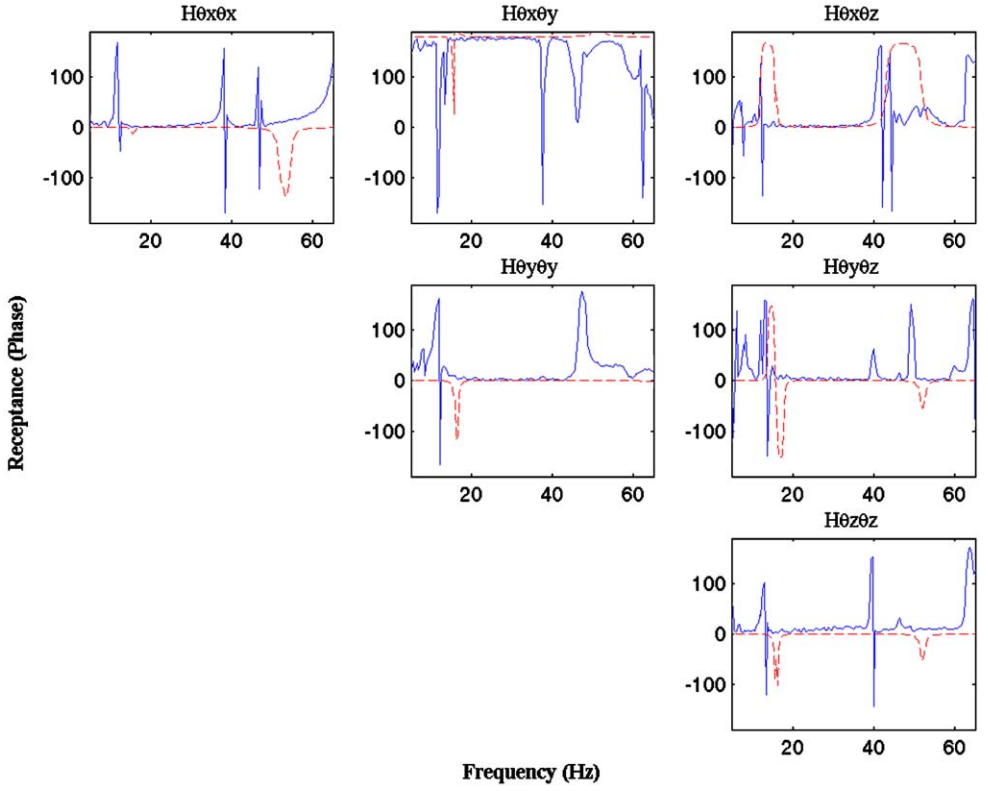

Fig. 11. Lower right-hand receptance matrix (phase): solid line—estimated from X-block measurements and dashed line—finite element.

The terms in Eq. (28) also appear in the transformation matrix **T**, so that the modification at the connection point is expressed in the form,

$$\Delta\mathbf{B} = -\omega^2\mathbf{T}^{\mathrm{T}}\Delta\mathbf{M}\mathbf{T} \tag{29}$$

and applied according to Eq. (26). The transformation matrix is written as,

$$\mathbf{T} = \begin{bmatrix} 1 & & 0 & r_z & -r_y \\ & 1 & -r_z & 0 & r_x \\ & & r_y & -r_x & 0 \\ & & 1 & & \\ & & & 1 & \\ & & & & 1 \end{bmatrix} = \begin{bmatrix} 1 & & 0 & 0.209 & 0.213 \\ & 1 & -0.209 & 0 & -0.256 \\ & & 1 & -0.213 & 0.256 & 0 \\ & & & 1 & & \\ & & & & 1 & \\ & & & & & 1 \end{bmatrix}. \tag{30}$$

This arrangement means that the mass modification is correctly located but connected by a single rigid link to the X-block connection point.

7. Modification results

A series of results are presented, beginning with a mass modification (without inertia) applied at the X-block connection point. Then the mass and inertia modification at the connection point ($\vec{\mathbf{r}} = 0$) is carried out. Finally, the complete modification including the full offset mass and inertia with position vector defined in Eq. (28) is considered.

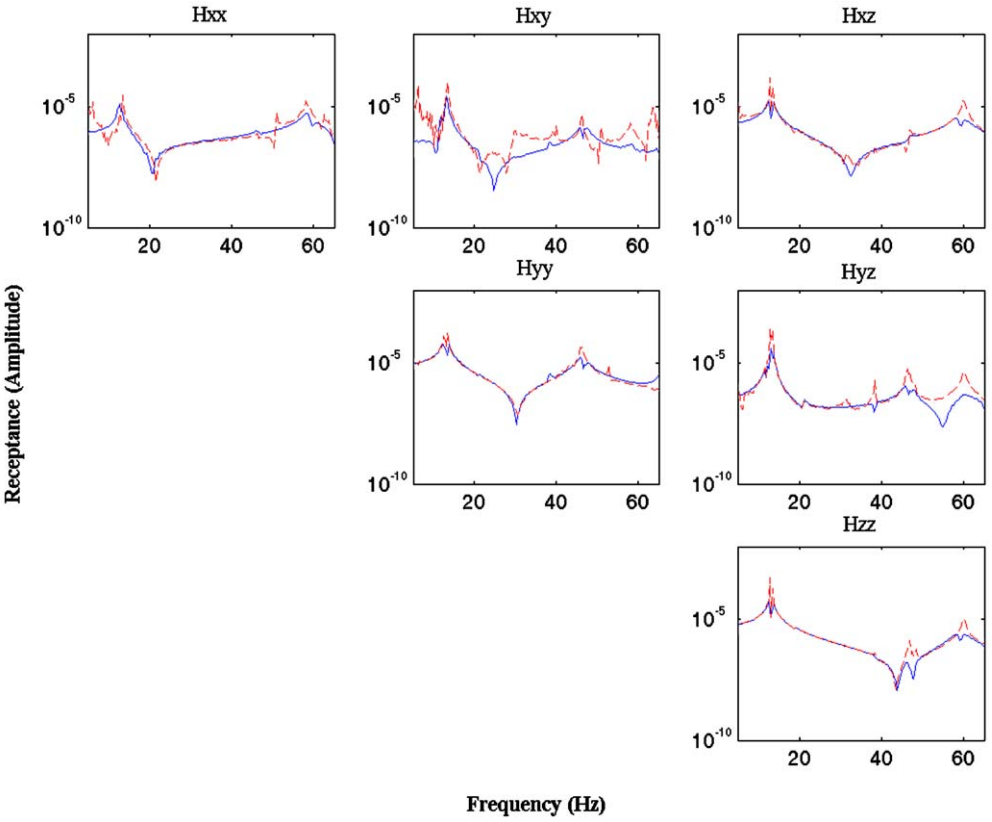

Fig. 12. Upper left-hand receptance matrix (magnitude—m/N): solid line—H_1 estimate and dashed line—H_2 estimate.

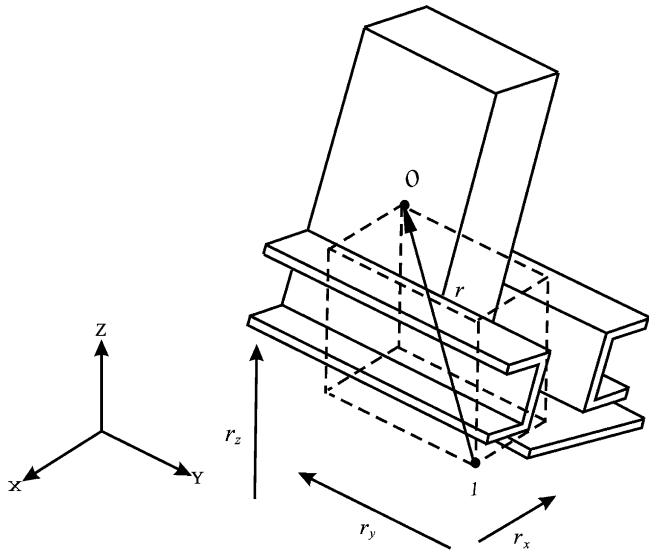

Fig. 13. Mass modification and position vector.

7.1. *Mass modification without inertia* ($\vec{\mathbf{r}} = 0$)

The results of the mass-only modification are shown in Fig. 15. The two sets of results, shown by the solid and dashed lines, are obtained by using the 6×6 receptance matrices shown in Figs. 6–11. The receptances

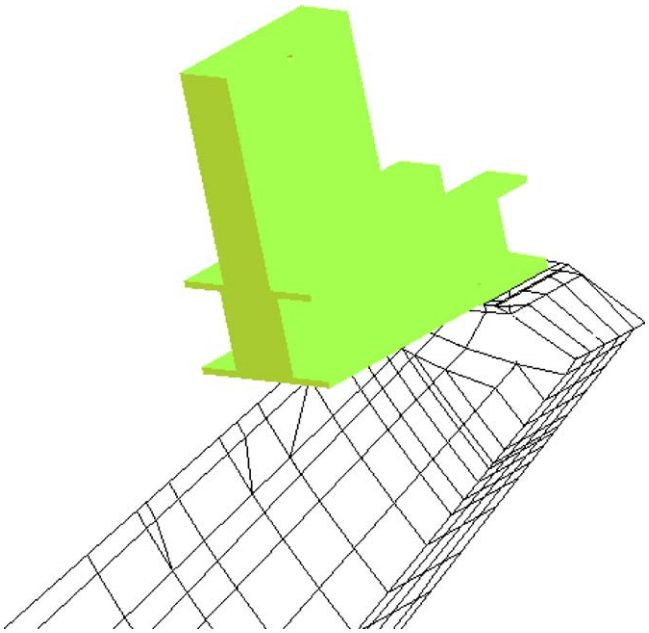

Fig. 14. Solid model and FE mesh.

given by the solid lines are determined by applying Eq. (26) to the measurements (solid lines) in Figs. 6–11. Correspondingly the dashed-line receptances shown in Fig. 15 are obtained by applying Eq. (26) to the finite-element (dashed-line) receptances in Figs. 6–11. The upper left-hand sub-matrix is sufficient to show that the main features of the two sets of receptances are very similar. As with the initial-system receptances the finite-element model is found to be stiffer than the physical tailcone.

7.2. *Mass modification with inertia* ($\vec{\mathbf{r}} = 0$)

It is seen from Fig. 16 that the effect of the inertia is significant. The prominent double measured peak at around 30 Hz in receptance h_{xy} shown in Fig. 15 has changed shape completely in Fig. 16. Note though, that the shapes of the diagonal-term receptances have not changed very much, except for a fairly modest reduction in the natural frequencies. This is because this modification with $\vec{\mathbf{r}} = 0$ does not introduce the strong coupling between the different motions of the tailcone that appear when the mass modification is overhanging.

7.3. *Full offset mass and inertia modification*

From the result shown in Fig. 17 it is apparent that the effect of the offset (overhang) is indeed very significant. The shapes of the receptances and the natural frequencies are all quite different to those shown in Fig. 16. There remains, however, good agreement in the general shape of the solid-line and dashed-line receptances shown in Fig. 17, although the noise that was apparent on the experimental solid lines in Fig. 16 has increased in magnitude on the solid-line receptances in Fig. 17. This is because the dynamic behaviour of modified system is now very different to that of the initial system, as can be seen by comparing Fig. 17 to Fig. 6. The modified receptances were obtained using Eq. (26), which requires the full 6×6 receptance matrix of the initial system, including the difficult to measure receptances such as the diagonal terms of the submatrix shown in Fig. 7, which were noticed previously to be noisy. This noise on the initial-system receptances is amplified in the data processing of Eq. (26) because the overhanging mass now causes the coupling of different tailcone motions that were virtually uncoupled in the initial system.

A vibration test was carried on the physically modified tailcone, but the receptances obtained were quite different from the experimental and finite-element results shown in Fig. 17. These separately obtained results,

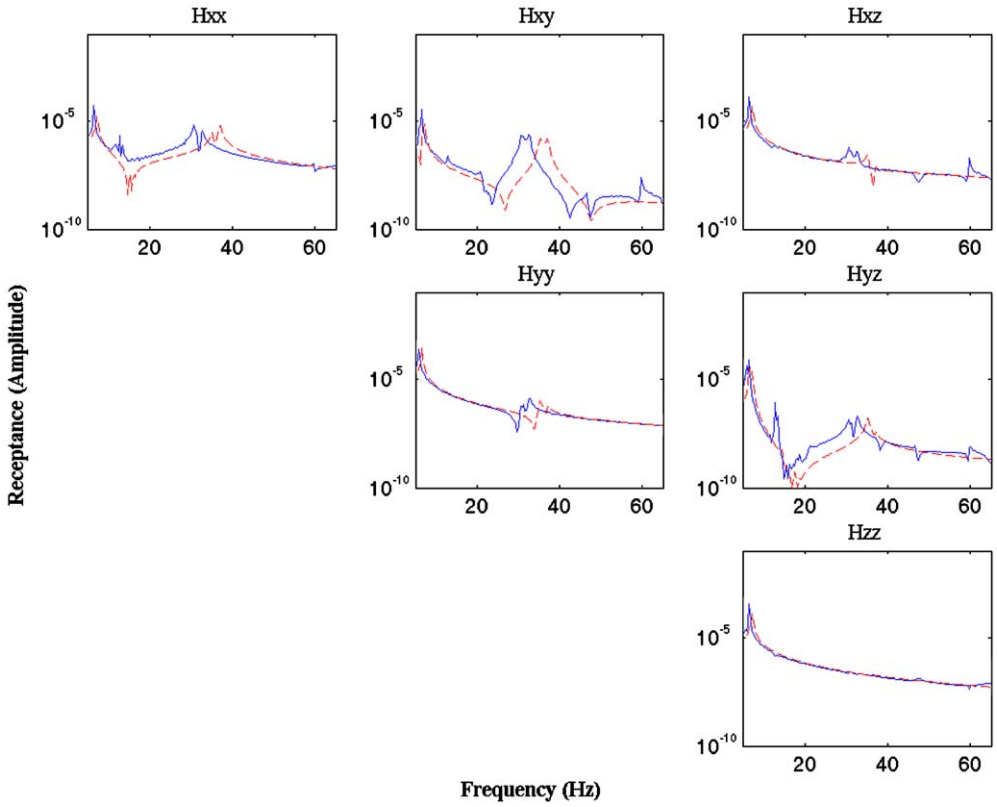

Fig. 15. Receptances (m/N)—mass-only modification: solid line—experimental and dashed line—finite element.

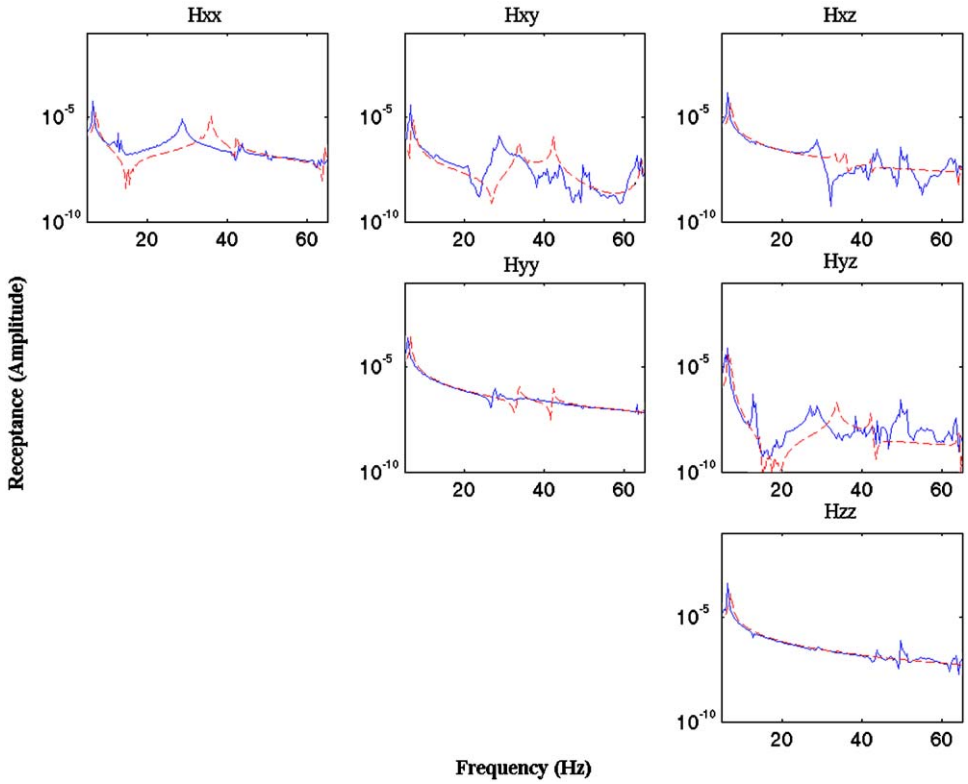

Fig. 16. Receptances (m/N)—mass and inertia modification ($\vec{\mathbf{r}} = 0$): solid line—experimental and dashed line—finite element.

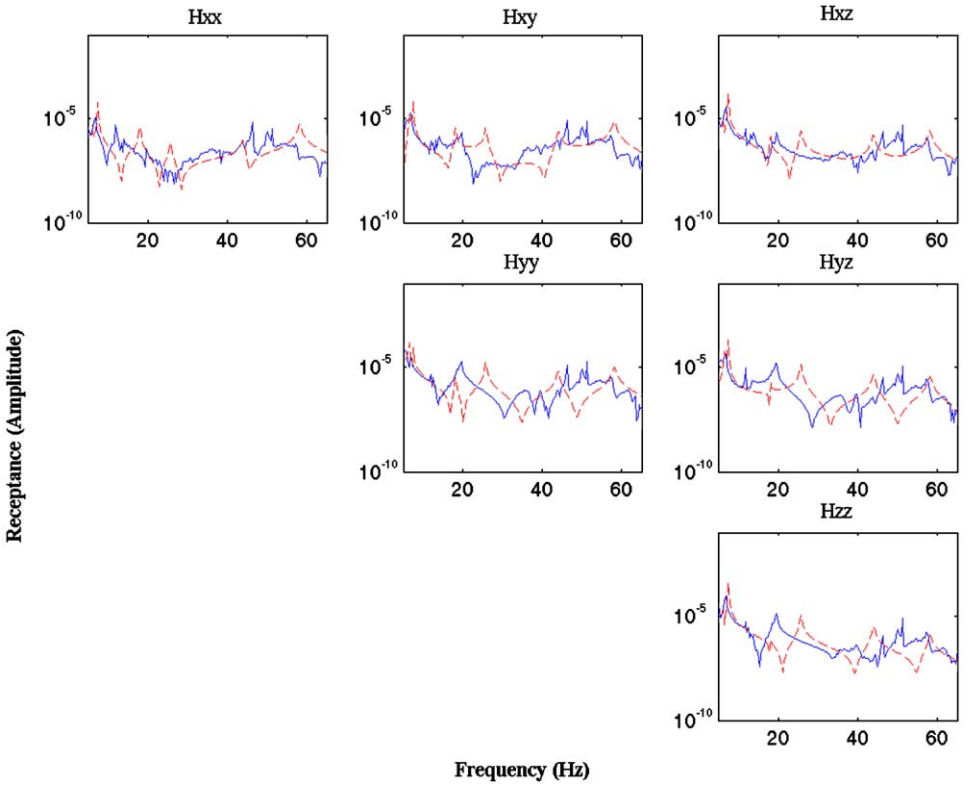

Fig. 17. Receptances (m/N)—full overhanging mass and inertia modification: solid line—experimental and dashed line—finite element.

from a hammer test, are given by the solid lines shown in Fig. 18. The reason for the difference between the two sets of results in Fig. 17 and the solid-line results in Fig. 18 becomes apparent when the overhanging mass is connected to the tailcone at several points instead of the single-point connection at the X-block attachment point. The dashed-line receptances shown in Fig. 18 were obtained using a multi-point constraint with 16 RBE2 (MSC-NASTRAN) elements. It may be seen that when the connection is representative of the real joint between the mass modification and the tailcone the resulting finite-element receptances are in good agreement with the hammer test results. The joint with multiple connections is clearly much stiffer that than the single-point rigid-connection joint, which shows many natural frequencies lower than they should be and introduces other natural frequencies not present in the experimental test. The MAC diagrams shown in Figs. 19 and 20, produced using 58 accelerometer measurements, show the improvement achieved by the multiple-point connection.

To apply the multiple-point connection using the receptance method would require the measurement of the full 6×6 receptance matrix at each of the connection points, and in this case there were six of them. This would be a task requiring great care and a significant amount of time. It might seem that one could take a single measurement and then assume a rigid connection to each of the other points, in this way producing the full 6×6 receptance matrix at each of the six connections. However, the centre of gravity of the modification would then be fixed by further rigid links to each of the connection points. Together all of these rigid connections would be defined in terms of the single original measurement, and therefore would be no different from what was done before and shown in Fig. 17. Close observation of Figs. 17 and 18 shows that only the first double peak close to 7 Hz is accurately determined by the rigid-connection assumption to a single X-block measurement. So, at the higher natural frequencies, the small differences in the receptances at close points where the modification is really connected to the tailcone are significant. Therefore to replicate the measurement shown in Fig. 18 it would be necessary to take measurements independently (and very accurately) at each of the connection points with an X-block. Despite the very good results shown in

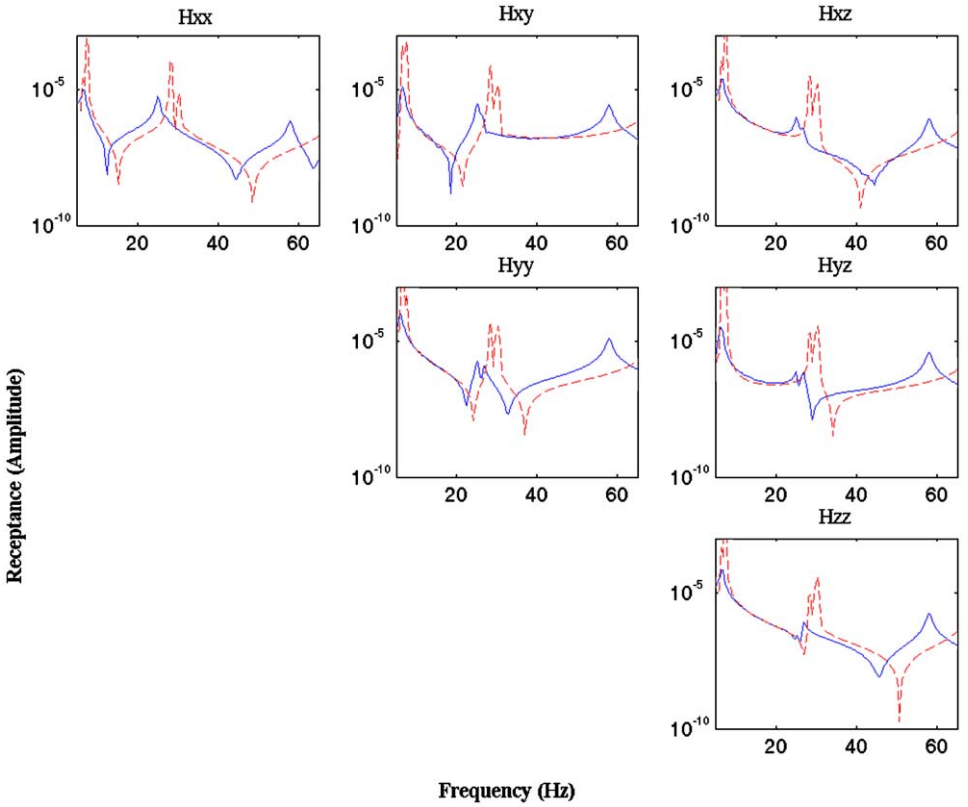

Fig. 18. Receptances (m/N): solid line—hammer test and dashed line—finite element with six RBE2 elements.

Figs. 6–11 it has to be doubted that sufficient accuracy can be achieved in the original measurements to allow the effects of the modification to be determined with sufficient accuracy because of noise amplification as demonstrated in Fig. 17.

8. A note concerning nonlinearity

It is known that certain structures, typically interconnected slender beams, may exhibit a form of behaviour, termed autoparametric, whereby small nonlinear interactions have a very considerable effect on forced vibration behaviour possibly leading, under internal resonance conditions, to the absorption of directly excited modes and large non-synchronous responses in modes that are not excited directly [10,11]. In its physical appearance the tailcone/pylon structure resembles the sort of structures that in other studies have shown this behaviour. However, the estimated X-block receptances, from wideband multi-frequency shaker excitation, did not show any significant nonlinearity although the averaging carried out in the estimation process would have had a linearising effect. The upper left-hand receptance matrix shown in Fig. 6 was measured at a number of different excitation levels without any significant deviation in the resulting linearised receptance estimates. The dynamic stiffnesses $\mathbf{B}_{11}(\omega)$, $\mathbf{B}_{10}(\omega)$, $\mathbf{B}_{00}(\omega)$, $\mathbf{B}_{01}(\omega)$ in Eq. (1) are not used explicitly so that in principle there is no assumption of linearity in the theory leading to Eq. (10) for the receptance $\mathbf{H}_{00}(\omega)$, which may be dependant upon response magnitude.

9. Conclusions

The structural modification theory enabling the estimation of the full 6×6 matrix of receptances using an X-block is presented. The X-block is represented by a finite-element model and included in the formulation of the H_1 and H_2 estimators. The former is shown to give superior results in tests carried out on a Westland Lynx

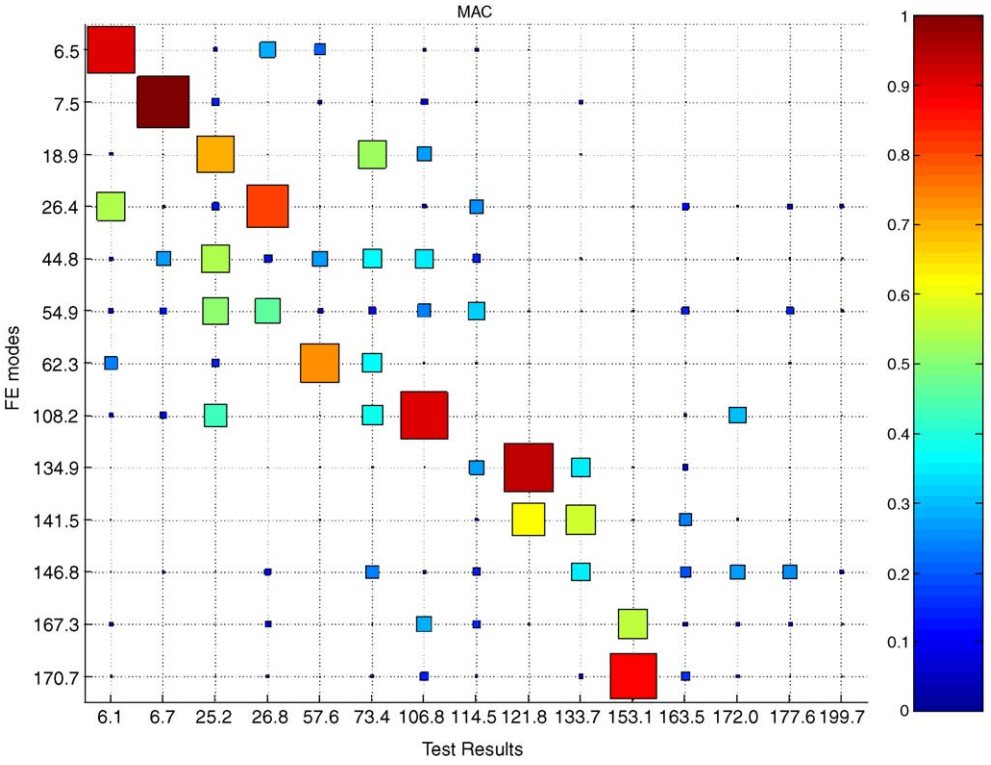

Fig. 19. MAC diagram: Single connection point.

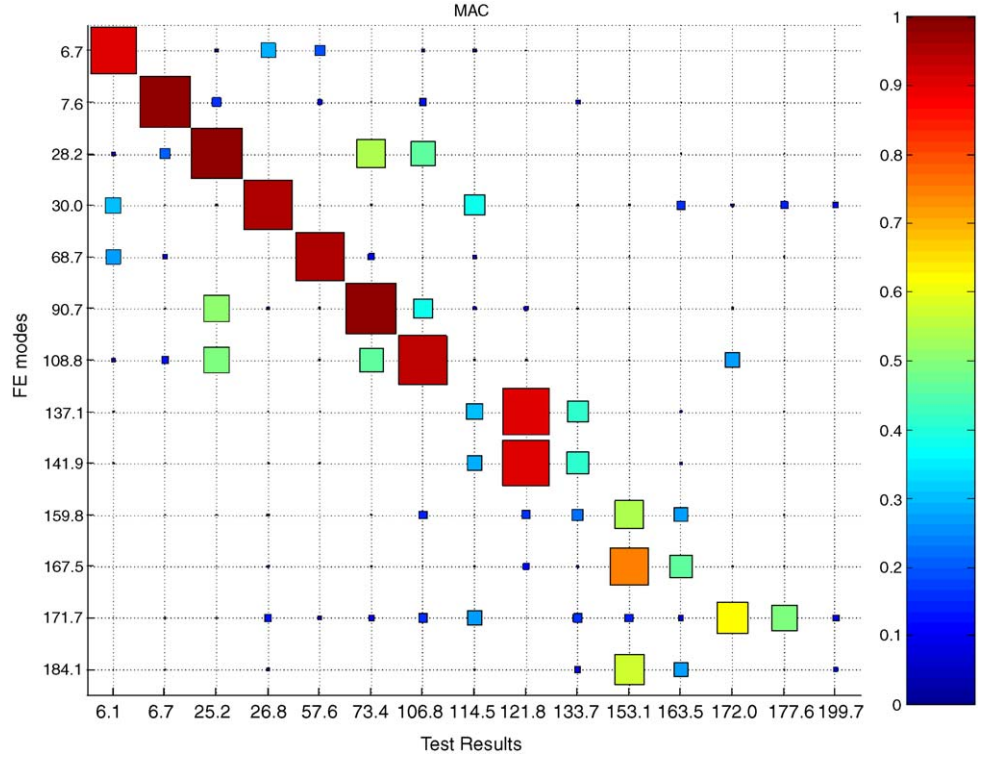

Fig. 20. MAC diagram: Multiple connections.

tailcone. The rotational receptances obtained using an X-block with the H_1 estimator show very good agreement with results from a finite-element model, the only significant difference being that the finite-element model is stiffer than the real structure. The 6×6 matrix of receptances includes terms that are extremely difficult to measure because the geometry of the tailcone is almost, but not quite, symmetric about the X–Z plane, so that very weak responses may be obtained to certain excitations. The modification, in the form of a large overhanging mass (representative of the tail-rotor gearbox and hub and of about the same mass as the baseline tailcone) has the effect of coupling all of the initial-system receptances. This has the effect of amplifying the noise of the weakly excited initial-system responses. At frequencies higher than the first double peak a single X-block measurement is insufficient to define the connection between the modification and the tailcone and it is shown, using the finite-element model, that further independent measurements are required to accurately determine the modified-system dynamics, including the overhanging mass and inertia. It is considered that the exercise carried out on the Lynx tailcone, with a very large overhanging mass modification and a near-symmetric initial structure, provides a very useful guide to the practical limitations of structural-modification theory.

Acknowledgments

The authors wish to acknowledge the provision of hardware, finite-element models and facilities by Westland Helicopters Ltd. and QinetiQ Ltd. The experiments described in the paper were carried out in the BLADE Laboratory by kind permission of the University of Bristol. The research was supported by EPSRC Grant GR/R43563. Ms. Ghandchi Tehrani is supported by an Overseas Research Students (ORS) award and a University of Liverpool Studentship.

References

[1] W.J. Duncan, The admittance method for obtaining the natural frequencies of systems, *Philosophical Magazine* 32 (1941) 401–409.
[2] R.E.D. Bishop, D.C. Johnson, *The Mechanics of Vibration*, Cambridge University Press, Cambridge, 1960.
[3] D.J. Ewins, *Modal Testing: Theory, Practice and Application*, second ed, Research Studies Press, Baldock, Hertfordshire, UK, 2000.
[4] J.E. Mottershead, Y.M. Ram, Inverse eigenvalue problems in vibration absorption: passive modification and active control, *Mechanical Systems and Signal Processing* 20 (1) (2006) 5–44.
[5] J.E. Mottershead, C. Mares, S. James, Fictitious modifications for the separation of close modes, *Mechanical Systems and Signal Processing* 16 (5) (2002) 741–755.
[6] J.E. Mottershead, A. Kyprianou, H. Ouyang, Structural modification, part 1: rotational receptances, *Journal of Sound and Vibration* 284 (1–2) (2005) 249–265.
[7] A. Kyprianou, J.E. Mottershead, H. Ouyang, Structural modification, part 2: assignment of natural frequencies and antiresonances by an added beam, *Journal of Sound and Vibration* 284 (1–2) (2005) 267–281.
[8] J.S. Bendat, A.G. Piersol, *Random Data: Analysis and Measurement Procedures*, Wiley, New York, 2000.
[9] G.V. Narayanan, On direct computation of beam dynamic stiffness computations using MSC-NASTRAN, MSC Software Corporation, Southfield, MI, USA.
[10] B.L. Bux, J.W. Roberts, Non-linear vibratory interactions in systems of coupled beams, *Journal of Sound and Vibration* 104 (3) (1986) 497–520.
[11] M.P. Cartmell, J.W. Roberts, Simultaneous combination resonances in a parametrically excited cantilever beam, *Strain* 23 (3) (1987) 117–126.